Diamond Films and Technology
Vol. 8, No. 4 1998
MYU Tokyo

DFT 189

Investigations of Surface Damage and Conduction Mechanisms During Field Emission from Chemical Vapor Deposited Diamond and Diamond-Like Carbon Films

Paul W. May, Stefan Höhn, Michael N. R. Ashfold,
Wang N. Wang*, Neil A. Fox*, Tim J. Davis* and John W. Steeds*

School of Chemistry, University of Bristol, Bristol BS8 1TS, U.K.
*Department of Physics, University of Bristol, Tyndall Avenue, Bristol BS8 1TR, U.K.

(Received 10 March 1998; accepted 21 May 1998)

***Key words*:** CVD diamond, field emission, damage sites, conduction mechanisms, Raman mapping

The field emission properties of undoped CVD diamond and DLC films prepared under different deposition conditions are measured. Scanning electron microscopy and laser Raman mapping are used to investigate the nature and appearance of the damage site after testing. These observations, together with the mathematical form of the observed current-voltage relations, are consistent with a model for the overall emission current combining conduction mechanisms through the bulk of the film with Fowler-Nordheim tunnelling at the surface.

1. Introduction

Electron emission from the surface of chemical vapor deposited (CVD) diamond and diamond-like carbon (DLC) films is of current interest due to potential applications in cold cathode devices. The negative electron affinity (NEA) of certain hydrogenated diamond surfaces plays an important role,[1] and the effect of different surface-terminating species can greatly affect the emission characteristics.[2] However, since most low field emission experiments use CVD diamond or DLC films with poorly characterized surfaces, it is clear that NEA is not solely responsible for the emission process. Other conduction mechanisms

become important as the charge carriers pass through different regions of the film from the electrode contact to the diamond surface. The two basic models for carrier injection at a metal-insulator interface or a metal surface are Schottky emission and Fowler-Nordheim injection.[3] In the bulk, other conduction mechanisms have been suggested, including space charge limited current (SCLC),[4] (which occurs in insulators at high applied field or high current densities), and Poole-Frenkel (PF) conduction,[5,6] which is basically a hopping mechanism. Other proposed mechanisms include PF with space charge limitation[7] (PF + SCLC), or PF with overlap of the coulombic potentials of the defect sites, known as Hill-type conduction.[5]

Bulk conductivity experiments performed on undoped CVD diamond films[8–11] have shown that the SCLC model can provide a good description of the dominant conduction mechanism. The magnitude of the space-charge currents in these experiments implies a band tail with a high density of states, increasing exponentially toward the valence band. The density of states measured in these experiments suggests that conduction occurs through highly disordered regions, such as the grain boundaries of polycrystalline films. As a result, grain boundaries have been proposed as the dominant conduction path in CVD diamond films.[12]

We report here the results of a series of field-emission experiments performed upon undoped microcrystalline CVD diamond and amorphous DLC films produced using a variety of deposition conditions. By observing the morphology of the damage site created by the field emission, and careful analysis of the mathematical form of the current-voltage dependence of the emission, insight into the conduction mechanisms in the various types of films can be obtained.

2. Experimental

CVD diamond films were deposited on Si (100) substrates that had been previously abraded with 1–3 μm diamond grit, using conditions typical for a hot-filament CVD reactor: process pressure 20 Torr, filament temperature 2300°C, substrate temperature 900°C, and growth rate 0.5 $\mu m\ h^{-1}$. Growth for 6 h give films that were 3 μm thick. The process gas was a mixture of CH_4 in H_2, with three methane concentrations. CH_4 (0.5%) produced high-quality polycrystalline diamond films of around 1 μm crystal size, CH_4 (1%) produced good-quality diamond with many grain boundaries and crystal size of around 0.5 μm, and CH_4 (2%) produced poor-quality 'ballas'-type diamond of around 0.05 – 0.1 μm crystal size.

DLC films were deposited on mirror-polished (100) Si using a 13.56 MHz radio-frequency parallel-plate reactor and CH_4 as the sole process gas. The process pressure was varied from 5–200 mTorr and the RF power from 10–300 W (DC self-bias 60–500 V) over an 8-cm-diameter electrode. Deposition time was 30 min, producing smooth, featureless DLC films of 0.1– 0.2 μm thickness. RF powers greater than about 70 W produced films that were hard, stressed and electrically insulating, and had a high degree of sp^3 character. With decreasing RF power, or increasing pressure, the films became softer and more graphitic, and were more electrically conducting.

The field-emission characteristics of the films were tested using a diode configuration

consisting of a cathode (the film under test) and a tungsten tip anode (cylindrical shape, 0.5 mm in diameter) mounted in a turbo-pumped vacuum chamber at a base pressure of 10^{-6} Torr. The tip-sample distance was continuously adjustable over a range of a few hundred μm. A negative voltage of up to 5 kV was applied to the cathode using a PC-controlled power supply, whilst the emission current was measured automatically as the voltage was ramped at a rate of ~50 V s^{-1}. A current limit of 0.2 mA was set to avoid destruction of the films by excessive current flow. To minimize the effects of run-to-run inconsistencies, in each case current-voltage (*I-V*) data were measured for three films that were deposited using identical conditions, and at two different places on each film. Values of the threshold voltage were calculated, and subsequent data analysis was performed, using the average of ten *I-V* curves measured at each position on each sample — an average of 60 data sets in all.

During testing, we found it necessary to ramp the voltage up and down several times in order to stabilize the *I-V* curves and to make them reproducible. This conditioning or activation effect has been reported previously,[13] and is often accompanied by morphological changes on the film surface. For both CVD diamond and DLC films, the nature and appearance of the damaged site varies depending on the properties of the film and the testing conditions. These damage sites are believed to occur as a result of extremely high local fields in the vicinity of the emission site causing dielectric breakdown of the surface, followed by rapid heating and evaporation of the surface layers.[14] The damage sites were studied by scanning electron microscopy (SEM) and laser Raman mapping (LRM). The latter technique was performed using a Renishaw Raman System 2000 incorporating an Ar ion laser operating at 488 nm.

3. Results and Discussion

3.1 *Electron emission damage in DLC and diamond films*

The damage arising from the emission sites on diamond and DLC films depends strongly on the deposition conditions and the electrical conductivity of the film. Studies on the evolution of these damaged areas[15] have suggested a possible formation mechanism whereby high current density travelling through the conduction pathways in the film (probably in the grain boundaries, see later) causes rapid local heating and evaporation of the surface layer. This leaves an indentation in the film surface, which deepens and widens as emission continues.

Typically, a damage site appears as shown in Fig. 1(a) for a DLC film deposited under medium power (say, 50 W). A number of equally spaced craters appear across the entire 0.5-mm-diameter tested area. For a DLC film produced at low RF power, i.e., a softer, more conducting, graphitic film, the density of the craters increases, often linking up to form enlarged areas (tens or hundreds of μm across) where the film no longer exists and only Si is visible (Fig. 1(b)). In the case of a DLC film deposited at powers lower than ~20 W, the crater density after field-emission testing was so high that the film over the entire 0.5-mm-diameter tested area was removed. Moreover, the exposed Si seemed much less damaged compared with the films deposited at higher RF powers, suggesting that this DLC film had either delaminated or burnt off so rapidly that the local heating effect of the high current density had no chance to significantly affect the underlying Si. This could be because the

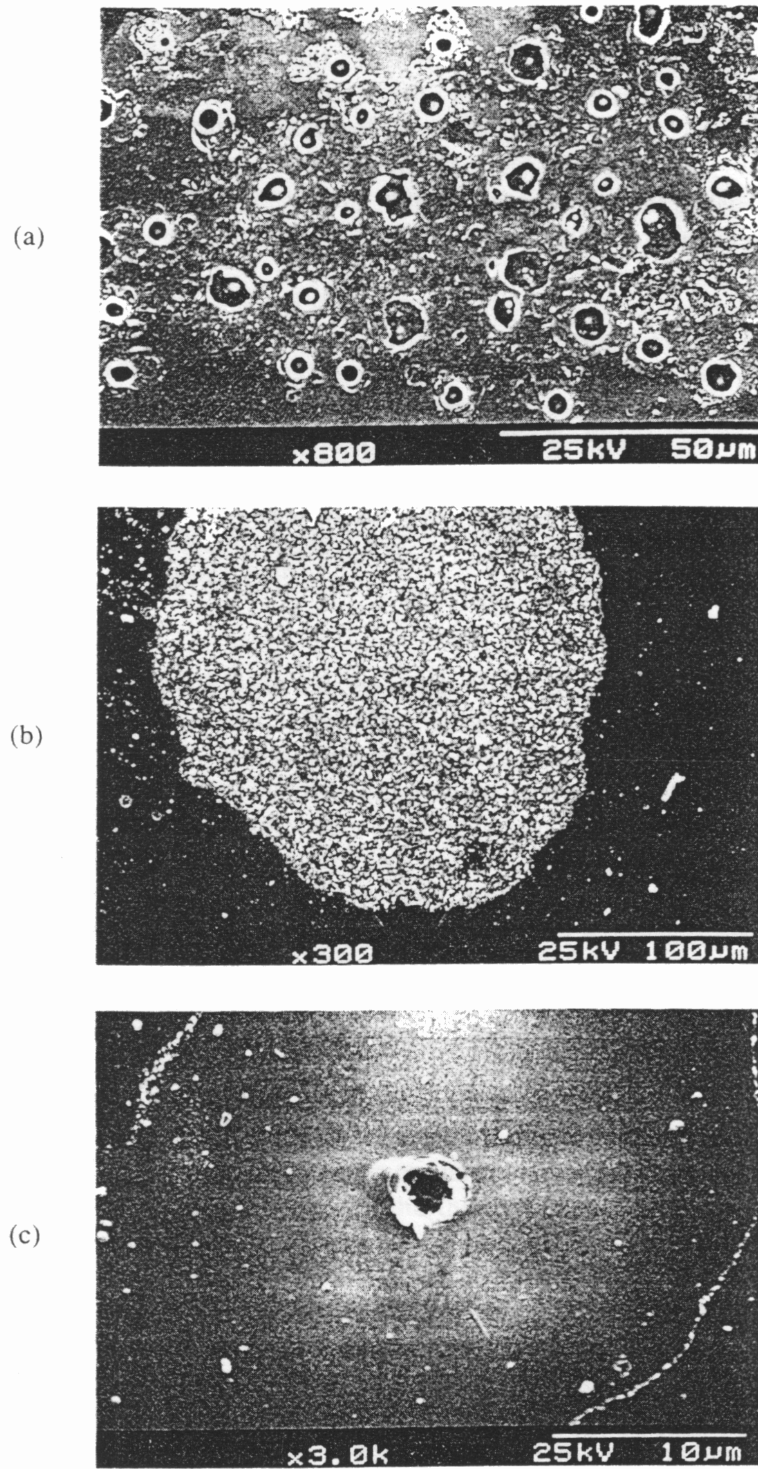

Fig. 1. Electron micrographs of the damage site in DLC films deposited at (a) 50 W, (b) 20 W and (c) 100 W, showing different types of cratering behaviour.

current density had been shared by many neighboring emission sites, reducing the local current density below that needed to melt and vaporize Si. Conversely, for DLC films produced at high RF powers (100 W), the crater density decreased, to ultimately form a single feature, located somewhere near the center of the tested area (Fig. 1(c)). This shows the opposite extreme, in that the entire emission current occurred at only one site, causing excessive and very localized heating and producing either a large, deep crater (often down to a depth of several μm into the Si substrate), or sometimes a hillock of melted and recrystallized C and Si materials.

For CVD diamond films, a similar trend to that above is observed, although not as pronounced. The ballas-type films grown with high methane concentration show damaged areas containing many linked craters, whereas the more crystalline, insulating films grown with low methane concentration show fewer, isolated craters. An example of an isolated, deep crater formed in a good-quality, insulating CVD diamond film is shown in Fig. 2. The similarity of these crater structures to the ones observed for DLC films suggests a common mechanism for their formation in both types of films. It also implies that the structure of a DLC film may be described in a similar fashion to that of CVD diamond, i.e. conducting channels embedded in an insulating matrix.[15]

3.2 *Laser Raman mapping*

Figure 3 shows the results of laser Raman mapping of the damage site shown in Fig. 2. The three maps (Figs. 3(a) – 3(c)) are displayed using suitable wavelength regions for diamond, graphite and Si, respectively. In Figs. 3(a) and 3(b), the center of the crater appears black, indicating the complete absence of diamond and graphite in this area. However, in Fig. 3(c), this area appears white due to the presence of Si. This shows that the film has been completely removed in this central region. Immediately surrounding the rim of the crater, we see enhanced signal intensity for graphite and Si, possibly resulting from the redeposition of evaporated material. Intensity due to graphite and Si can still be seen at distances greater than 0.25 mm from the edge of the crater, but now the diamond intensity also increases, suggesting that the thickness of the obscuring layer is decreasing. Figure 3(d) shows the laser Raman intensity map of the variation of the full width at half-maximum (FWHM) of the diamond line. It can be seen that at the edge of the crater, the FWHM of the line increases from 6 cm^{-1} to 8 cm^{-1}, indicating an increase in disorder as the diamond becomes more damaged. A similar map of the absolute position of the diamond peak (not shown) showed no variation across the sample, with the peak having a constant value of 1336 cm^{-1}. This shows that the diamond is under some tensile stress, but that this stress does not change near the crater edge. Figure 4 shows the laser Raman spectra taken from different positions around the damage site. Figure 4(a) is taken at a distance of 0.5 mm from the crater rim: it shows a strong diamond signal, as well as the G-band of graphite centered around 1550 cm^{-1}. The Si peak at ~520 cm^{-1} arises from both the underlying substrate and the redeposited Si. Figure 4(b) is taken from the edge of the crater rim: it shows a small Si peak as well as the graphite D-band. No diamond peak is seen. Finally, Fig. 4(c) is taken from the center of the crater, and shows the presence of only the Si peak. The asymmetry of the peak implies that silicon is either nanocrystalline or semi-amorphous, and that a morphological change has occurred during crater formation.

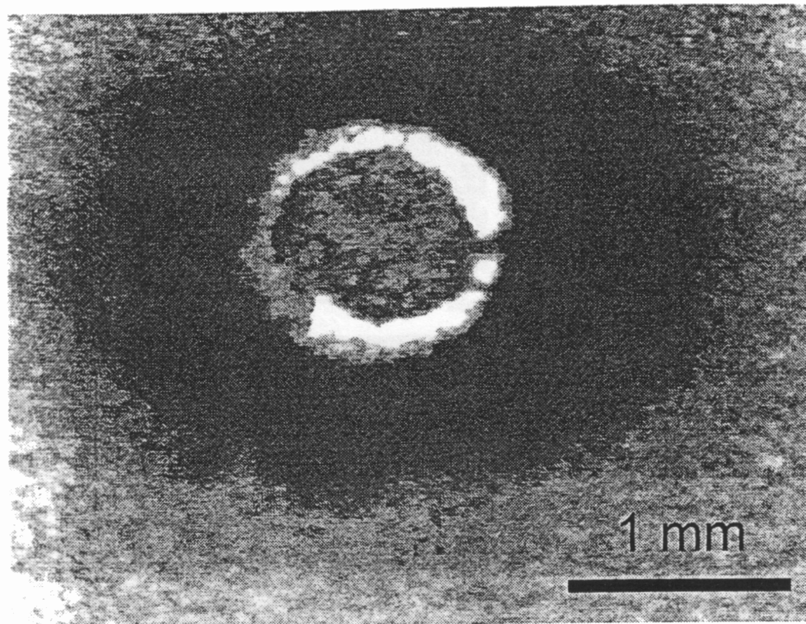

Fig. 2. White light optical microscope image of the damage site observed after field-emission testing of an undoped CVD diamond film grown with 0.5% CH_4 in H_2. The current drawn was 100 μA for 60 min. The entire 1-mm-diameter tested area was destroyed and the film completely removed, with a blackened area extending at a large distance away from the crater.

3.3 *Field-emission results*

When discussing field emission, the most commonly used model for the ejection of electrons from a surface is the well-known Fowler-Nordheim equation.[3] However, this model only deals with surface or interface effects, and there are many other models for the mechanisms of conduction in the bulk of insulators[11] which may be important when studying field emission from diamond. The expected current-voltage relations for some of these models are given in Table 1. By plotting the appropriate mathematical form of these relations as abscissa and ordinate, a straight-line plot can be obtained. The correlation coefficient of the best fit line gives a direct measure of how well each model fits the experimental data. An example of each of these types of plots for one of the samples is given in ref. 15, and Table 2 lists the results of such analyses for each of the CVD and DLC films investigated.

Starting with the DLC films, we find that for the more conducting, softer DLC films, the Fowler-Nordheim model gives a better fit than any of the other models (except for, perhaps, the SCLC model that gives comparable results). However, as the films become harder and more insulating, some of these other models, in particular, the Schottky emission, SCLC, and SCLC + PF models, provide increasingly better fits to the data, although the Fowler-Nordheim model is still the best choice. For very insulating films (*e.g.*, the one grown at 90 W RF power), these other models provide as good a fit to the data as the Fowler-Nordheim

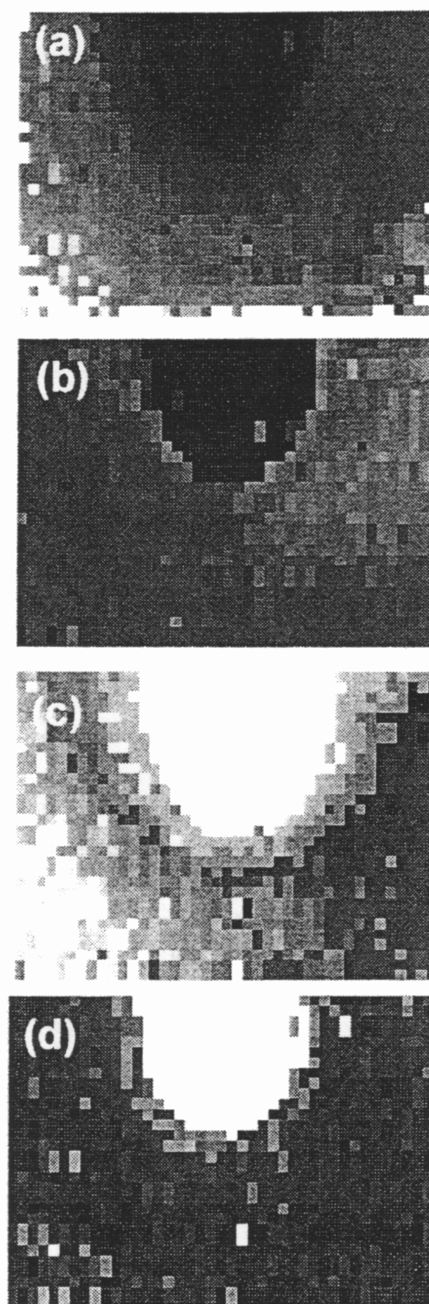

Fig. 3. Laser Raman intensity maps of the lower half of the damage site shown in Fig. 2, taken with a resolution of 25 μm. The size of the mapped area is 0.5 mm high by 1 mm across. The maps are viewed using selected Stokes shift wavelength regions for (a) diamond (1330–1340 cm^{-1}), (b) graphite (1450–1700 cm^{-1}) and (c) Si (510 – 530 cm^{-1}), with an intensity scale whereby white indicates high-intensity signals at that point. Plot (d) shows a map of the variation of the FWHM of the diamond line, scaled so that black and white correspond to 6 cm^{-1} and 8 cm^{-1}, respectively.
Note: due to a feature of the data collection software, the center of the crater in (d) appears white even though there is no diamond signal intensity from this region.

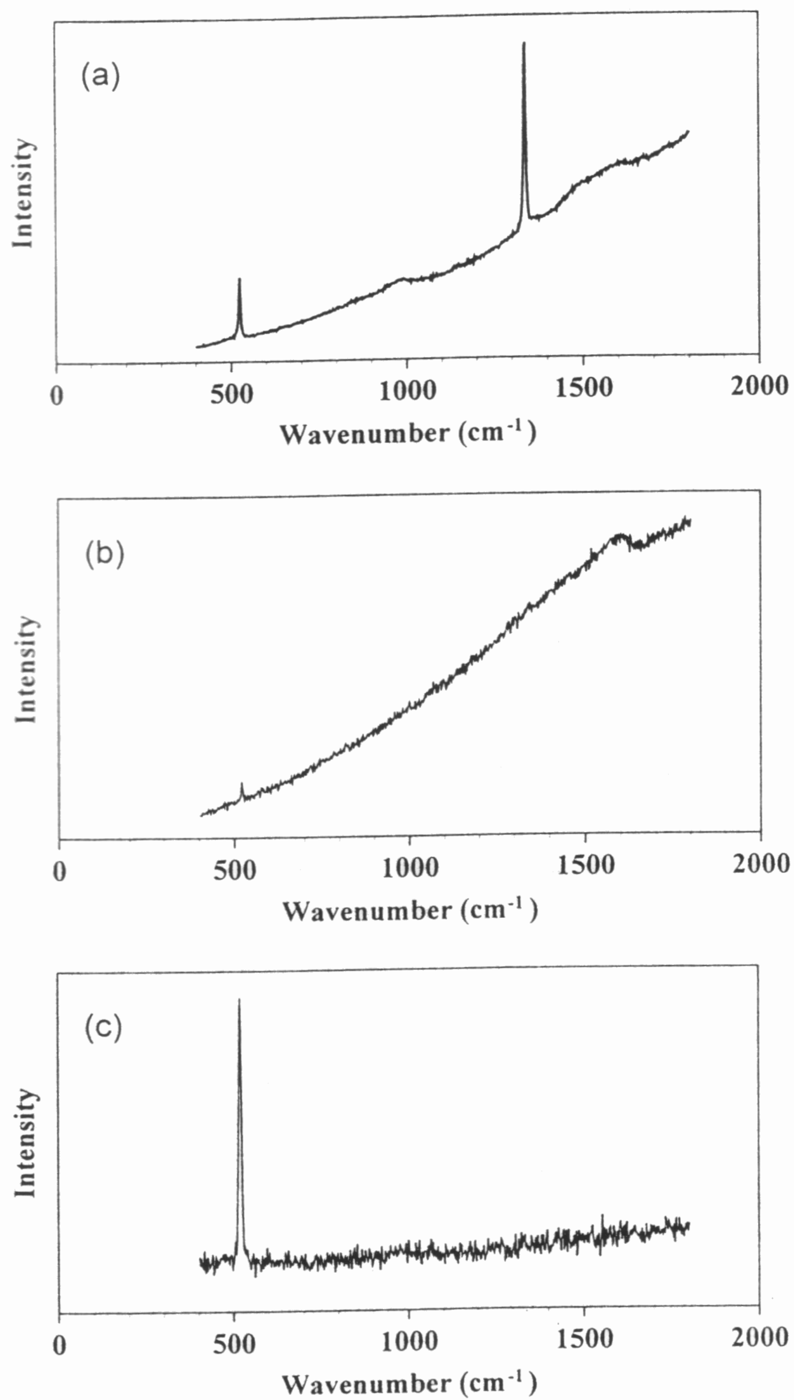

Fig. 4. Laser Raman spectra (488 nm) taken from different positions around the damage site shown in Fig. 2. (a) About 0.5 mm from the crater rim with the diamond peak visible, (b) from the edge of the crater rim, showing peaks from both Si and graphite, but not diamond, and (c) at the center of the crater, showing only the presence of the Si peak.

Table 1
The most usual mechanisms of conduction in insulators, their expected current-voltage relations[11] and mathematical relations required for a straight-line plot.[16]

Type of conduction	Current-voltage relation	Ordinate	Abscissa
1) Shottky emission	$I \sim \exp(aV^{1/2}/kT)$	$\ln I$	$\sqrt{V}$
2) Fowlder-Nordheim	$I \sim V^2\exp(-a/V)$	$\ln(I/V^2)$	$1/V$
3) SCLC	$I \sim V$ (low fields)	I	V
	$I \sim V^n$ ($n > 1$, high fields)	$\ln I$	$\ln V$
4) SCLS + PF	$I \sim V^2\exp(aV^{1/2}/kT)$	$\ln(I/V^2)$	$\sqrt{V}$
5) PF	$I \sim V\sinh(aV^{1/2}/kT)$	$\sinh^{-1}(I/V)$	$\sqrt{V}$
6) Hill's law	$I \sim \sinh(aV/kT)$	$\sinh^{-1} I$	V

Table 2
Threshold voltages (V_{th}) and correlation coefficients (r^2) for the best fit straight lines of the different data plots given in Table 1 for various CVD diamond and DLC films. For the PF and Hill's Law plots, a straight-line fit was inappropriate because the plots were obviously curves, giving r^2 values < 0.7 in each case, so these have been omitted. To reduce scatter due to random error, the values for each film are averages from up to 60 sets of I-V data, as described in the text. Our estimated uncertainty for each of the quoted threshold voltages is ± 4 V μm^{-1}, whilst the values for the correlation coefficients are reproducible to two decimal places.

		r^2 values for different conduction models			
	V_{th}/V μm^{-1}	Fowler-Nordheim	Schottky	SCLC	SCLC + PF
CVD 0.5% CH_4	38	0.95	0.99	0.99	0.99
CVD 1% CH_4	25	0.96	0.99	0.98	0.98
CVD 3% CH_4	19	0.99	0.96	0.98	0.94
DLC 30 W	43	0.93	0.90	0.92	0.85
DLC 50 W	31	0.98	0.93	0.96	0.92
DLC 60 W	29	0.98	0.92	0.96	0.88
DLC 90 W	60	0.99	0.99	0.99	0.98

model. In no case did the standard PF or Hill's Law models produce a straight line, and so the mechanisms implied by these two models can be ruled out as being significant for DLC films.

This trend is also observed in CVD diamond films, although the differences are not clear cut: films grown using methane-rich conditions are best modelled by the Fowler-Nordheim equation, whereas for better quality films, other models perform as well, if not better. Indeed, for high-quality CVD films grown using 0.5% CH_4, the Schottky emission, High-

Field SCLC and SCLC + PF models appear to provide much better descriptions of the overall conduction mechanism than the Fowler-Nordheim model.

A possible explanation for these observations can be made using arguments based on the conductivity of the film. For films with high conductivity, only the tunnelling of the electrons through the potential barrier is significant, since conduction through the film would be relatively facile. For highly insulating films, however, conduction through the bulk of the film might become potentially rate-limiting. Thus, bulk conduction mechanisms (such as SCLC), as well as mechanisms occurring at various interfaces (such as Schottky emission), may begin to play a significant role in electron transport. If this is true, the observed current-voltage dependence will be well modelled by a combination of these mechanisms and the Fowler-Nordheim surface ejection model.

4. Conclusions

In conclusion, the observations presented here have given an insight into the mechanisms by which emission causes breakdown and destruction of undoped CVD diamond and DLC films, as well the conduction processes occurring in these films. For highly insulating diamond and DLC films, electrical conduction through the film bulk is a process that should not be overlooked, since it contributes to the overall observed emission characteristics. A study of the temperature dependence of the field-emission current may also provide more evidence of the nature of the conduction mechanisms that are important in these films. The ease with which diamond and DLC films become damaged during field emission may have implications on the lifetime of field emission devices. However, the relevance of this to the more highly doped, and therefore highly conducting films, which are likely to be used when fabricating real devices, is still unclear. More work needs to be done, therefore, to study the effects of diamond doping level on field emission and crater formation. The effect of substrate conductivity is also an area that needs attention.

Acknowledgments

PWM wishes to thank the Royal Society for financial support and the award of a University Research Fellowship. SH thanks the Socrates & Youth Technical Assistance Office of the EU for financial help. The authors would also like to thank David Pickard for some of the laser Raman work.

References

1) C. Bandis and B. B. Pate: Appl. Phys. Lett. **69** (1996) 366.
2) P. W. May, J. C. Stone, M. N. R. Ashfold, K. R. Hallam, W. N. Wang and N. A. Fox: Diamond. Relat. Maters. **7** (1998) 671.
3) J. J. O'Dwyer: *The Theory of Electrical Conduction and Breakdown in Solid Dielectrics* (Clarendon, Oxford, 1973).
4) M. A. Lampert and P. Mark: *Current Injection in Solids* (Academic, New York, 1970).
5) R. M. Hill: Philos. Mag. **23** (1971) 59.

6) Y. Muto, T. Sugino, J. Shirafuji and K. Kobashi: Appl. Phys. Lett. **59** (1991) 843.
7) P. N. Murgatroyd: J. Phys. D: Appl. Phys. **3** (1970) 151.
8) S. Ashok, K. Srikanth, A. Badzian, T. Badzian and R. Messier: Appl. Phys. Lett. **50** (1987) 763.
9) J. Mort, M. A. Maconkin and K. Okumura: Appl. Phys. Lett. **59** (1991) 455.
10) M. Werner, O. Dorsch, A. Hinze, E. Obermeier, R. E. Harper, C. Johnston, P. R. Chalker and I. M. Buckley-Golder: Diamond and Relat. Mater. **2** (1993) 825.
11) P. Gonon, A. Deneuville, F. Fontaine and E. Gheeraert: J. Appl. Phys. **78** (1995) 6633.
12) B. Fiegl, R. Kuhnert, M. Ben-Chorin and F. Koch: Appl. Phys. Lett. **65** (1994) 371.
13) N. A. Fox, W. N. Wang, T. J. Davis, J. W. Steeds and P. W. May: Appl. Phys. Letts. **71** (1997) 1.
14) R. Hessmer, M. Schreck, S. Geier and B. Stritzker: Diamond Relat. Maters. **3** (1994) 951.
15) P. W. May, S Höhn, M. N. R. Ashfold, W. N. Wang, N. A. Fox, T. J. Davis and J. W. Steeds: J. Appl. Phys. **84** (1998) 1618.
16) P. W. May, S. Höhn, W. N. Wang and N. A. Fox: Appl. Phys. Letts. **72** (1998) 2182.